

Detection of single molecules using stochastic resonance of bistable oligomers.

Anastasia Markina*, Alexander Muratov, Vladislav Petrovskii, and Vladik Avetisov*

N. N. Semenov Federal Research Center for Chemical Physics Russian Academy of Sciences, Kosygina 4, 119991 Moscow, Russia; icp@chph.ras.ru

* Correspondence: markina@mpip-mainz.mpg.de (A.M.), vladik.avetisov@gmail.com (V.A.)

Received: date; Accepted: date; Published: date

Abstract: Ultrasensitive elements for nanoscale devices capable of detecting single molecules are in demand for many important applications. It is generally accepted that the inevitable stochastic disturbance of a sensing element by its surroundings will limit detection at the molecular level. However, a phenomenon exists (stochastic resonance) in which the environmental noise acts abnormally - it amplifies, rather than distorts, a weak signal. Stochastic resonance is inherent in nonlinear bistable systems with criticality at which the bistability emerges. Our computer simulations have shown that the large-scale conformational dynamics of a short oligomeric fragment of thermoresponsive polymer, poly-N-Isopropyl-methacrylamid, resemble the mechanical movement of nonlinear bistable systems. The oligomers we have studied demonstrate spontaneous vibrations and stochastic resonance activated by conventional thermal noise. We have observed reasonable shifts of the spontaneous vibrations and stochastic resonance modes when attaching an analyte molecule to the oligomer. Our simulations have shown that spontaneous vibrations and stochastic resonance of the bistable thermoresponsive oligomers are sensitive to both the analyte molecular mass and the binding affinity. All these effects indicate that the oligomers with mechanic-like bistability may be utilized as ultrasensitive operational units capable of detecting single molecules.

Keywords: thermoresponsive oligomers, nanomechanics, bistability, stochastic resonance, single molecules detection.

1. Introduction

The desire to build the detecting, control, and logic elements as small as possible actively stimulates the search for molecular structures of nanometer size capable of performing discrete operations at the molecular level. To date, impressive advances have been made in mastering various nanodevices, e.g., switches [1,2], sensors [3-6], catalytic agents [7], actuators [8], and logic gates [9]. Submicron-sized mechanical and electromechanical machines are also an important advance [10-14]. However, the design of molecular machines a few nanometers in size remains a challenge.

A nanometer-sized molecule must have a specific dynamic in order to work as a machine. Indeed, such a molecule, being large enough, has a huge number of degrees of freedom. However, machine-like action implies low-dimensional dynamics, which are supposed to be realized through collective atomic motions associated with the one or two slowest degrees of freedom of the molecule. To be distinguished dynamically, the functional degrees of freedom must be separated from all faster degrees of freedom by a large spectral gap [15-17]. Therefore, the search for molecular structures performing machine-like action is severely limited.

The very type of operation can further narrow the scope of the search. Switching, for example, implies an abrupt change in state of a two-state system when the controlling stimulus crosses a threshold value. In terms of dynamical systems, switching is a nonlinear dynamic with criticality [18,19].

A commonplace metal ruler subjected to longitudinal compression is a simple demo system with critical behavior. Indeed, the ruler remains straight under light compression. However, as soon as the compressive force exceeds a certain critical value, the straightened state becomes unstable and the ruler bends up or down. Above critical compression, the ruler is a bistable dynamical system and can jump from one state to another. In dynamical terms, the compression transforms one-state dynamics into bistable dynamics, which are characterized by potential energy with two minima separated by a bistability barrier. The ability of a metal plate to abrupt changes in states via applied power loads is exactly what is used in mechanical switches.

Bistability is interesting not only for the discrete action. If random perturbations can activate transitions over the bistability barrier, the bistable system will spontaneously jump between two states, performing spontaneous vibrations. The time intervals separating spontaneous jumps, i.e., the lifetimes of the system in each of two states, are widely distributed around a mean value, which, in turn, depends exponentially on the ratio of the bistability barrier to the intensity of the perturbation [20,21]. The exponential dependence enables the transformation of spontaneous vibrations into regular jumps via a slight wiggle of the bistable potential by a weak oscillating force. Regularization of spontaneous vibrations by a weak oscillating force was called stochastic resonance [20], mainly because the output associated with noise-induced transitions of the bistable system can be much larger than the weak oscillating force used as the input. In this sense, one can say that the stochastic resonance is a phenomenon involving the amplification of a weak signal by the noise. That is why the stochastic resonance has attracted much interest, in particular, for sensing [22,23].

In macroscale dynamical systems, the bistability barrier is macroscopically high, so the spontaneous vibrations of the macroscopic-sized bistable systems, e.g., of the micron- or even submicron-sized, cannot be activated by the thermal-bath fluctuations. Much stronger perturbations are needed. However, thermal fluctuations can be the major perturbations for systems a few nanometers in size. Therefore, if a nanometer-sized molecule is bistable, and if its bistability barrier is comparable to the thermal-bath

fluctuations energy, the spontaneous vibrations and stochastic resonance will appear naturally. Thermally activated spontaneous vibrations and stochastic resonance seem to be highly attractive for measuring at the molecular level.

Searching for mechanic-like bistability among molecules a few nanometers in size may not seem promising, but computer simulations give some hope [24]. Our intensive molecular dynamic simulations of rather short oligomeric fragments of thermoresponsive polymer poly-N- isopropyl-methyl-acrylamide (PNIPMA) subjected to longitudinal compression revealed specific oligomeric samples that successfully combine the nanometer size and mechanic-like bistability. These oligomers do exhibit thermally activated spontaneous vibrations and stochastic resonance, and both of these modes of bistability turned out to be sensitive to the attachment of single molecules. In this article, we present the computer simulation data on the mechanic-like bistability of a syndiotactic N-isopropylmethylacrylamid oligomer with a length of 30 units (oligo-30s-NIPMAm), as well as the data on the sensitivity of the oligomer spontaneous vibrations and stochastic resonance to the attachment of single molecules.

2. Materials and Simulation Methods

The simulation approach consists of the following steps: (i) equilibrium conformation of oligo-30s-NIPMAm below and under critical temperature ($\sim 32^\circ\text{C}$); (ii) application of a compression force to a closed 30s-NIPMAm conformation to observe spontaneous vibrations; (iii) application of external periodic stimuli to a critical compression force to observe stochastic resonance; (iv) addition of an analyte to 30s-NIPMAm to show a sensing regime.

We started with morphology simulations using the GROMACS simulation package [25]. In our approach, we first adapted the OPLS-AA force-field [26-28]. Because all Lennard-Jones parameters were taken from the OPLS-AA, the combination rules and the fudge-factor of 0.5 were used for 1–4 interactions. The long-range electrostatic interactions were treated by using a smooth particle mesh Ewald technique. All calculations were performed in the NVT ensemble using the canonical velocity-rescaling thermostat, as implemented in the GROMACS simulation package. The oligo-30s-NIPMAm and the environmental water were modeled in a fully atomistic representation in the box of size $8.0\times 8.0\times 8.0$ nm with a time step of 1 fs. The temperature was set at 290 K, i.e., the temperature sufficiently below the low critical solution temperature of the poly-NIPMAm [29-31].

The second step was a simulation of spontaneous vibrations. For that, we applied a longitudinal load. After the definition of a critical force for observing spontaneous vibration, we applied a weak oscillating force. Computational details of the application of longitudinal load and weak oscillation force for the oligomer in the free and sensing regime are described in Supplementary Materials, Note S1-S2.

3. Results

In this section, we describe a set of specific characteristics of the oligo-30s-NIPAM dynamics, which unambiguously show that the oligomer subjected to power loads behaves like a nonlinear system with criticality. Mechanic-like bistability, spontaneous vibration, and stochastic resonance are the focus of our simulations. In addition, we present the data corresponding to the sensitivity of the spontaneous vibrational and stochastic resonance modes of the oligomer to the attachment of single molecules.

3.1. Oligomeric templates for molecular dynamic simulations

We started with simulations of the molecular dynamics of oligo-30s-NIPAM at different temperatures to ensure that the oligomer was thermoresponsive, i.e., it actually had two well-defined conformational states (called, hereafter, "open" and "closed" states) and sharply changed the states when the temperature crossed a critical value. The oligomer states were characterized by the distance between the oligomer ends, while the oligomer conformation was additionally controlled by the gyration radius. The low critical solution temperature of the oligo-30s-NIPAM was specified to be close to 305 K [29-31], so the temperature equal to 290 K was chosen for the preparation of samples in the open state, while it was equal to 320 K for samples in the close state. Figure 1a shows the shapes of the open and closed states of oligo-30s-NIPAM equilibrated at 290 K and 320 K, respectively. The fluctuations of the end-to-end distance, Re , at these two states are shown in Figure 1b.

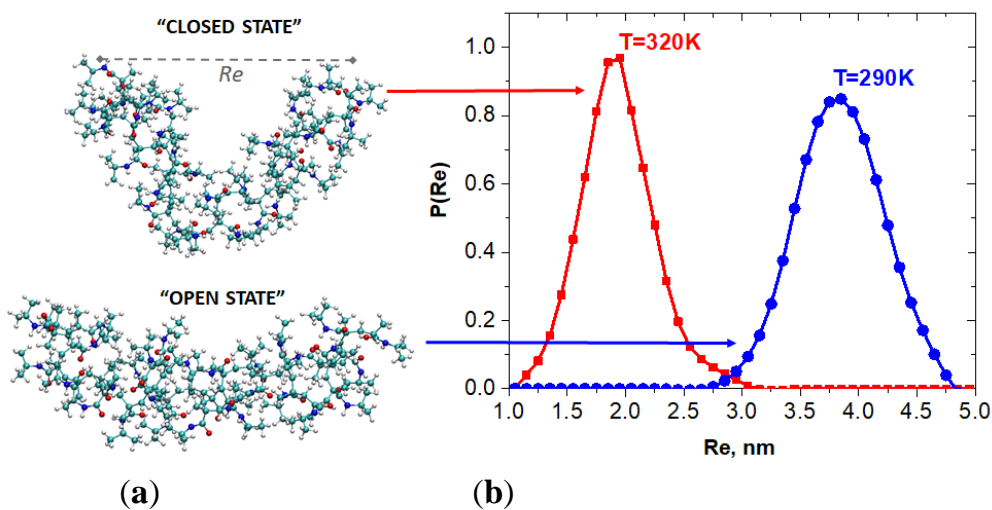


Figure 1. Temperature-induced bistability of the oligo-30s-NIPAM. (a) Typical shapes of the oligomer in the "open" and "closed" states equilibrated at the temperatures $T=290$ K and $T=320$ K, respectively; (b) Normalized distributions of fluctuations of the end-to-end distances Re at the open and closed states.

3.2. Bistability and spontaneous vibrations

Assuming that a longitudinal compression of the oligomer could lead to a sharp transition from the open state to the closed state as the compression exceeded a critical value, we took the oligomer equilibrated in the open state (at 290 K) and applied a

longitudinal compressive force, F , in the same manner as in the demo-ruler above (Figure 2a). In fact, one could take the oligomer equilibrated in the close state at 320 K and apply the pulling forces. Such experiments also were checked, and the results were qualitatively the same.

Figure 2b shows how the stationary states of the oligomer evolve when the compression grows.

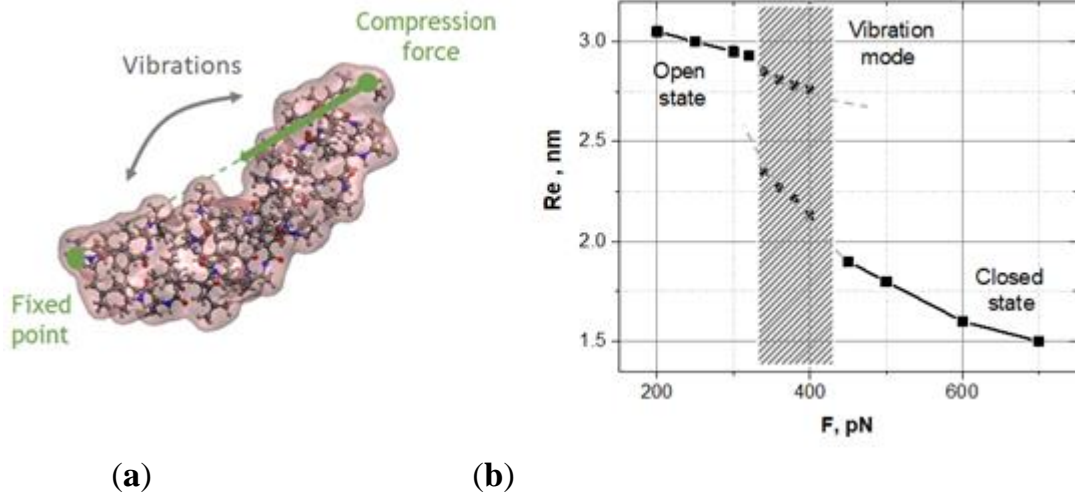


Figure 2. The response of the oligo-30s-NIPMAm to longitudinal compressions: (a) Schematic presentation of the oligomer compression; (b) The bifurcation diagram represents how the stationary states, Re , of the oligomer depend on compression F as a control parameter. A shadow interval of compression forces from 340–430 pN marks the area of spontaneous vibrations.

One can clearly see a drastic change in the oligomer dynamics near the critical point $F_c \approx 320$ pN. Indeed, the open state remains the only state of the oligomer up to the critical compression. However, at the critical compression, a new branch of actually bent stationary states appears. Far from the critical point, the oligomer is found in the open or closed state, depending on compression. If the compressive force quickly crossed the critical point, then the oligomer would abruptly transite from the open state to the closed state, like a jump-like switching of a metal ruler. Somewhat above the critical compression, low-frequency spontaneous vibrations between the open and closed states are observed, i.e., the oligomer is bistable in this region. It should be noted that spontaneous vibrations are not observed just after the critical point, despite the fact that there are two branches of states. Spontaneous vibrations are observed with some offset from the critical point, i.e., in the region where the bistability barrier matches the thermal fluctuations. The bistability barrier should be neither too small nor too large relative to thermal fluctuations.

To more accurately verify the spontaneous vibrations, we plotted the probability distributions, $P(Re)$, of the states Re averaged over a set of dynamic trajectories, $Re(t)$, and studied how these distributions were transformed when the compression grew. The bifurcation diagram in Figure 2b is reconstructed exactly from these data. Below and fairly above the bifurcation point $F_c \approx 320$ pN, the oligomer dynamics are characterized by single-pick distributions $P(Re)$ at the open or closed state, respectively. Near the bifurcation point

from above, there is an interval of compressions in which the distributions $P(R_e)$ have a double-peak form caused by spontaneous vibrations of the oligomer between the open and closed states. In our simulations, the mean lifetime of the states, i.e., the mean value of random time intervals between the jumps defined along dynamic trajectories, ranged from 5–10 ns, depending on the compression. Using Kramer's exponential relation between the lifetime of the states and the bistability barrier, and assuming that the pre-exponent collision factor is equal to 10^{-13} s, the bistability barrier was estimated as 10–15 $k_B T$, where k_B is the Boltzmann constant and T is the bath temperature. Following this estimate, we assumed that the reordering of hydrogen bonds between the oligomer and surrounding water could activate spontaneous vibrations of the oligo-30s-NIPMAm. If this were the case, the spontaneous vibrations would be caused precisely by the thermoresponsibility of the oligo-30s-NIPMAm, e.g., due to the switching of hydrogen bonds from the oligomer-water configuration to the oligomer-oligomer configuration [30,31].

To verify whether the mechanic-like spontaneous vibrations of the oligomer were, indeed, controlled by reversible switching of some hydrogen bonds, we checked the hydrogen bonds in the oligomer-water configuration and in the oligomer-oligomer configuration and studied how the number of these hydrogen bonds fluctuated. We realized that only the hydrogen bonds located in the oligomer bending area had a reasonable relation to the oligomer spontaneous vibration. These data are shown in Figure 3a.

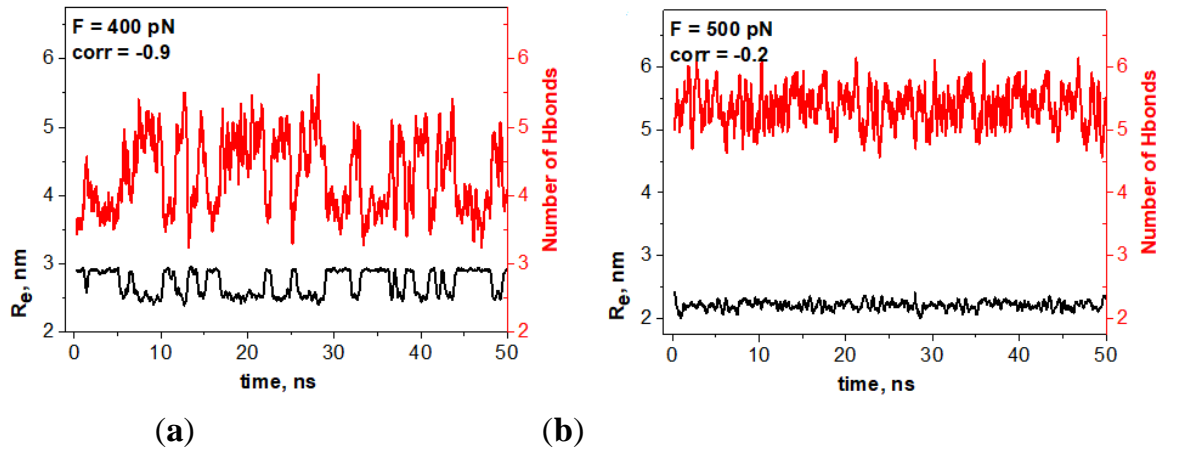


Figure 3. Correlation between the oligomer dynamics $R_e(t)$ and switching of hydrogen bonds located in the oligomer bending area. The compressions F are indicated on the panels. (a) Spontaneous vibrations of the oligomer (black curves, left axes, R_e nm) strongly correlate with the switching of hydrogen bonds from the oligomer-oligomer configuration to the oligomer-water configuration and back (red curves; right axes). (b) No significant correlation between the oligomer dynamics and the fluctuations of hydrogen bonds is seen beyond the bistability region.

One can see that spontaneous vibrations of the oligomer and the switching of particular hydrogen bonds are synchronized on antiphase with high correlation coefficients of -0.90. Figure 3b demonstrates that no significant correlation between the oligomer dynamics and the switching of hydrogen bonds is observed beyond the bistability region.

3.3. Stochastic resonance

Taking the oligomer in the spontaneous vibrations regime, we stimulate the stochastic resonance by applying an additional weak oscillating force directed along the compressive force F . The oscillating force was induced by external oscillating electrical field $E=E_0\cos\omega t$ acted on a charge (+1) set at one end of the oligomer, while a compensative charge was set at the opposite end. Following the well-known fact that the main resonance peak arises when the frequency of the oscillating field matches the mean value of the state lifetimes in the spontaneous vibrations mode [23], we tested the oci fields with the period of $T=5$ ns (200 MGz in frequency); the amplitudes ranged from 0.1 V/nm to 1.0 V/nm. For more details, see Supplementary Materials, Note S1.

The explicit manifestation of stochastic resonance induced by the oscillating force with the frequency of 200 MHz and the amplitude of 0.2 V/nm is shown in Figure 4.

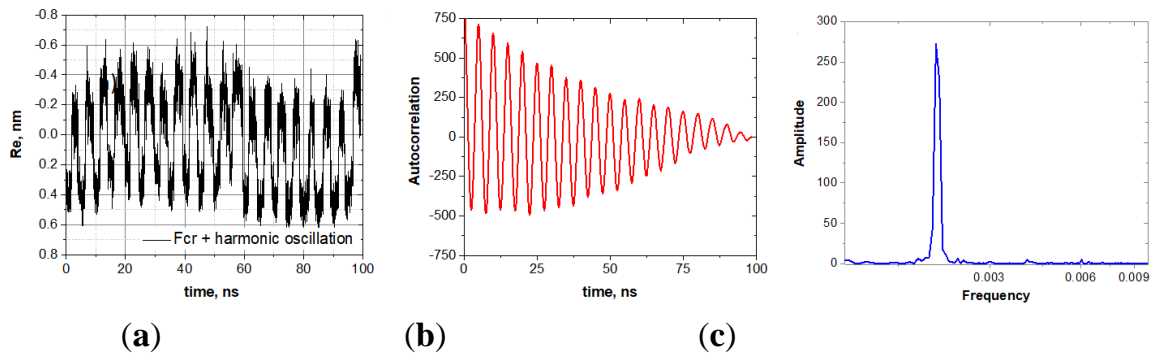
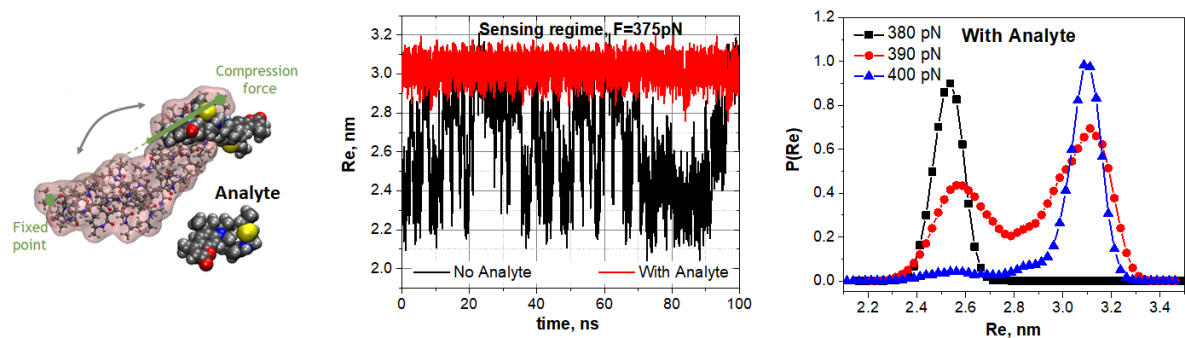


Figure 4. Stochastic resonance generated by harmonic electric field $E=E_0\cos\omega t$ with the amplitude 0.2 V/nm and the frequency 200 MGz: (a) The oligomer dynamic $Re(t)$ in the stochastic resonance mode; (b) The autocorrelation function of $Re(t)$; (c) The frequency spectrum of the autocorrelation function shown on panel (b).

3.4. Single molecules sensing via spontaneous vibrations mode

This series of computer experiments aimed to study the bistable dynamics of the 30s-NIPMAm when a molecular cargo was attached. It is known that nonlinear systems are sensitive to weak impact precisely near the bifurcation point [32-34]. Therefore, we first initiated the spontaneous vibration of unloaded oligo-30s-NIPMAm near the critical compression and then studied how the oligomer dynamics changed with molecular cargo attachment.

Figure 5 shows the response of spontaneous vibrations of the oligo-30s-NIPMAm at the compression of 375 pN to the attachment of a dye molecule (ATTO 390).



(a) (b) (c)

Figure 5. Sensitivity of the oligo-30s-NIPMAm spontaneous vibrations to the attachment of a single-molecule cargo (an analyte). (a) Schematic presentation of the computer experiments. (b) Spontaneous vibrations of the unloaded oligomer (black trajectory) at the compression of 375 pN, and non-vibrating dynamics of the oligomer loaded by an analyte at the same compressing force (red trajectory). (c) Evolution of statistical weights for visiting the open and closed states by the loaded oligomer vs. the compressive force. Molecular cargo (an analyte) shifts the spontaneous vibrations mode from the compression of 375 pN (see panel (b)) to the compressive of 390 pN.

Recall that the unloaded oligomer subjected to the same compression is bistable and vibrates spontaneously. However, as Figure 5b shows, the oligo-30s-NIPMAm escapes the spontaneous vibrations mode when a molecular cargo attaches to the oligomer. The loading by a cargo shifts the bistability region. This fact is additionally confirmed by the evolution of statistical weight distributions for visiting the open and closed states when the compressing force is varied. In particular, the attachment of a dye molecule shifts the compression under which the spontaneous vibrations are observed from 375 pN to 390 pN (Figure 5c). Note that a molecular cargo shifts the spontaneous vibrations mode toward the higher compression of the oligomer. The shifts must depend on the type and number of the molecules attached. The shifts of the spontaneous vibrations mode caused by the attachment of various molecular cargos are presented in Supplementary Materials, Note S2.

3.4. Single molecules sensing via stochastic resonance

Taking the oligomer in the spontaneous vibrations mode at the compression of 375 pN, we first initiated the stochastic resonance mode by applying an additional oscillating field $E = E_0 \cos \omega t$ with the amplitude $E_0 = 0,2$ V/nm and frequency $\omega = 2\pi/5$ ns⁻¹ and then studied how the oligomer dynamics changed with a molecular cargo attachment.

The spontaneous vibrations mode (red curve) and the stochastic resonance mode (black curve) for the oligomer without an analyte are shown in Figure 6a.

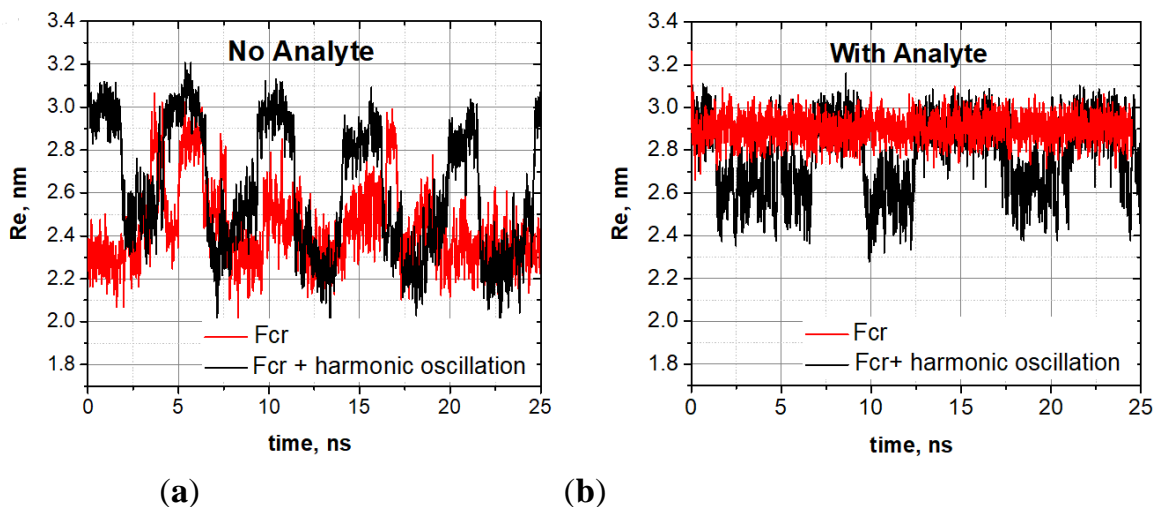


Figure 6. Stochastic resonance and the sensing regime. (a) Spontaneous vibrations (red curve) and stochastic resonance (black curve) of the unloaded oligo-30s-NIPMAm under the compression of 375 pN. (b) Dynamics of the oligomer loaded by a tryptophan molecule at the same conditions. Trajectories are marked as in panel (a).

In the spontaneous resonance mode, the oligomer itself responded to the oscillating force with the resonance frequency. The oligomer dynamics loaded by a molecular cargo are shown in Figure 6b. One can see that, when the cargo is attaching, the oligomer completely leaves the spontaneous vibrations mode (Figure 6b). The stochastic resonance mode is lost too, but the oligomer still vibrates, though the vibrations are not well-synchronized with the external harmonic field. These experiments showed that the attachment of a molecular cargo transformed the stochastic resonance mode into irregular jumps characteristic of spontaneous vibrations.

To see this transformation more clearly, we slightly increased the compressive force up to 390 pN and first generated the stochastic resonance of the oligo-30s-NIPMAm without a molecular cargo by applying the harmonic field of the amplitude $E_0 = 0,2$ V/nm and frequency $\omega = 2\pi/5$ ns⁻¹. Then we attached an analyte and generated new trajectories. The analyte-induced transformation of the stochastic resonance mode is clearly seen in a comparison of these two sets of trajectories, shown in Figure 7.

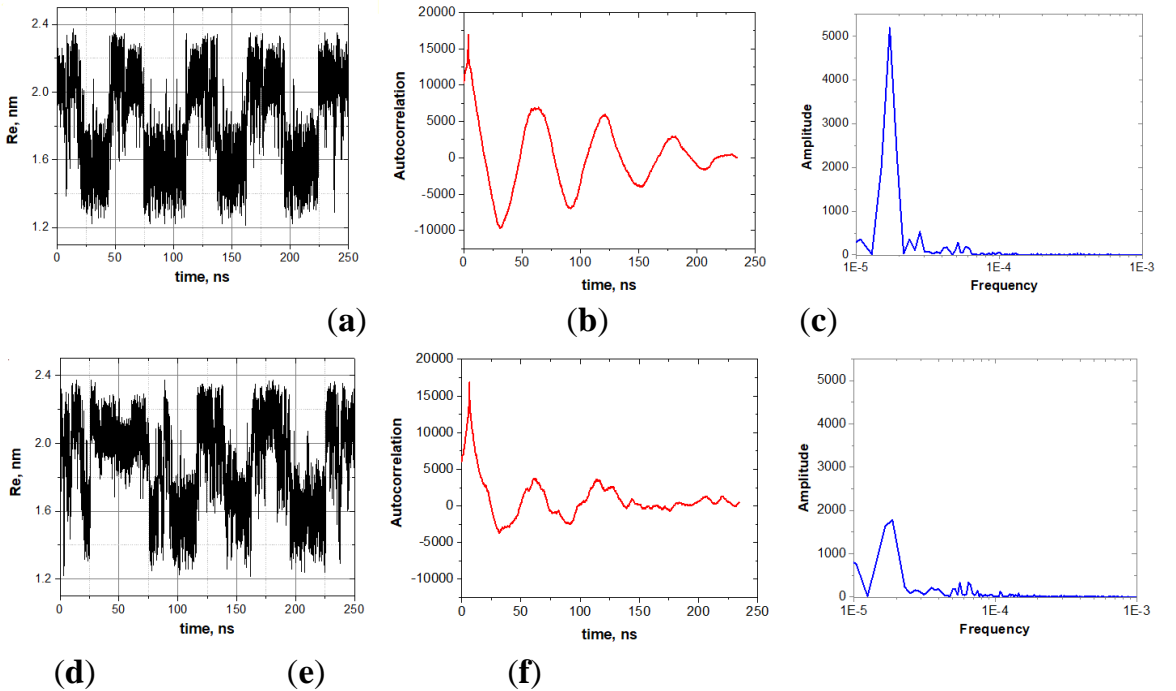


Figure 7. The analyte-induced transformation of the stochastic resonance mode. Vibrations of the oligo-30s-NIPMAm before (top row of panels) and after (bottom row of panels) the attachment of a tryptophan molecule: (a) – (c) Stochastic resonance mode of the oligo-30s-NIPMAm, its autocorrelation function, and the frequency spectrum. (d) – (f) Distortion of the spontaneous resonance mode caused by the attachment of a molecular cargo to the oligomer.

Summarizing this set of computer experiments, we conclude that the attachment of a molecular cargo can manifest itself in different ways.

4. Discussion

In most sensing applications, it is generally accepted that the inevitable stochastic disturbance imparted by the surroundings limits the detection signal at the molecular level. However, noise can be leveraged to amplify rather than distort a weak signal – a phenomenon known as stochastic resonance. Our computer simulation studies of nanometer-sized oligomeric fragments of thermoresponsive polymer poly-N-isopropyl-methyl-acrylamide subjected to longitudinal compression have shown that the large-scale conformational dynamic of the oligomers can exhibit non-linear dynamics similar to the dynamics of bistable mechanical systems. Besides the spontaneous vibrations and stochastic resonance, which in our case are activated by conventional thermal noise, these dynamic modes turn out to be sensitive to single molecule attachment. When a molecular cargo attaches, the stochastic resonance mode is blurred, or the resonance is transformed into the spontaneous vibrations mode, or the oligomer completely exits the vibrational mode. It is important that the spontaneous vibrations and stochastic resonance of the bistable oligomers are sensitive to both the analyte's molecular mass and its binding affinity (for more details, see Supplementary Materials, Note S3). All these effects manifest themselves to a sufficiently significant extent to be used in detecting the masses of single molecules in solutions. Therefore, bistable oligomers can act as ultrasensitive material capable of detecting single molecules against the background of natural stochasticity at the molecular level. Due to the small size of the oligomers, the stochastic resonance visibly shifts even when the attached molecule is about 200 Dalton in mass. This is sufficient for the detection of single molecules, e.g., hormones we have used as an analyte in our studies.

Importantly, the oligo-30s-NIPMAm that we established in this article is not a unique sample. Several oligomers of thermosensitive polymers have properties suited for exhibiting nano-mechanical bistability and detecting small molecules.

Acknowledgments: The authors acknowledge the Molecular Machine Corporation Ltd. for organization and support of the Molecular Machines Project.

References

1. Bazargan, G.; Sohlberg, K. Advances in modelling switchable mechanically interlocked molecular architectures. *International Reviews in Physical Chemistry* **2018**, 37:1, 1-82. DOI: 10.1080/0144235X.2018.1419042

2. Luo, Q.; Guo, Zh.; Zhang, Sh; et al. Crackbased complementary nanoelectromechanical switches for reconfigurable computing. *IEEE Electron Device Letters* **2020**, *41*(5), 784-787. DOI: 10.1109/LED.2020.298373
3. Zhou, X.; Lee, S.; Xu, Z. C.; Yoon, J. Recent Progress on the Development of Chemosensors for Gases. *Chem. Rev.* **2015**, *115*, 7944–8000. DOI: 10.1021/cr500567r
4. McConnell, A. J.; Wood, C. S.; Neelakandan, P. P.; Nitschke, J. R. Stimuli-Responsive Metal-Ligand Assemblies. *Chem. Rev.* **2015**, *115*, 7729–7793. <https://doi.org/10.1021/cr500632f>
5. Lou, Z. R.; Li, P.; Han, K. L. Redox-Responsive Fluorescent Probes with Different Design Strategies. *Acc. Chem. Res.* **2015**, *48*, 1358–1368. <https://doi.org/10.1021/acs.accounts.5b00009>
6. Tamayo, J.; Kosaka, P. M.; Ruz, J. J.; San Paulo, A.; Calleja, M. Biosensors based on nanomechanical systems. *Chem. Soc. Rev.* **2013**, *42*, 1287-1311. <https://doi.org/10.1039/C2CS35293A>
7. Van Dijk, L.; Tilby, M. J.; Szpera, R.; et al. Molecular machines for catalysis. *Nature Reviews Chemistry* **2018**, *2*, 0117–0120. <https://doi.org/10.1038/s41570-018-0117>
8. Liang, J.; Huang, L.; Li, N.; Huang, Y.; Wu, Y.; et al. Electromechanical Actuator with Controllable Motion, Fast Response Rate, and High-Frequency Resonance Based on Graphene and Polydiacetylene. *ACS NANO* **2012**, *6*(5), 4508-4519. <https://doi.org/10.1021/nn3006812>
9. Akarvardar, K.; Wong, H.-S. P. Nanoelectromechanical Logic and Memory Devices. *ECS Transaction* **2009**/ *19*, 49–59.
10. Ekinici, K. L.; Roukes, M.L. Nanoelectromechanical systems. *Rev. Sci. Instr.* **2005**, *76*, 6, 061101-061112. <https://doi.org/10.1063/1.1927327>
11. Zhang, L.; Marcos, V.; Leigh, D. Molecular machines with bio-inspired mechanisms. *Proc. Nat. Acad. Sci. USA* **2018**, *115*, 9397–9404. DOI: 10.1073/pnas.1712788115
12. Cleland, A. N. Foundation of Nanomechanics. From Solid-State Theory to Device Applications. Springer-Verlag: Berlin Heidelberg, Germany, 2003. DOI <https://doi.org/10.1007/978-3-662-05287-7>
13. Eoma, K.; Park, H. S.; Yoon, D. S.; Kwon, T. Nanomechanical resonators and their applications in biological/chemical detection: Nanomechanics principles. *Physics Report* **2011**, *503*, 115-163. DOI:10.1016/j.physrep.2011.03.002
14. Krakover, N.; Ilic, B. R.; Krylov, S. Displacement sensing based on resonant frequency monitoring of electrostatically actuated curved micro beams. *J. Micromech. Microeng.* **2016**, *26*, 115006-11017. DOI:10.1088/0960-1317/26/11/115006
15. Hansen, J. C.; Skalak, R.; Hoyer, A. An elastic network model based on the structure of the red blood cell membrane skeleton. *Biophys. J.* **1996**, *70*, 146–166. DOI:10.1088/0960-1317/26/11/115006
16. Togashi, Y.; Mikhailov, A. S. Nonlinear relaxation dynamics in elastic networks and design principles of molecular machines. *Proc. Natl. Acad. Sci. USA*. **2007**, *104*, 8697–8702. DOI:10.1073/pnas.0702950104

17. Düttmann, M.; Mittnenzweig, M.; Mikhailov, A. S. Complex intramolecular mechanics of G-actin - An elastic network study. *PLoS ONE* **2012**, 7(10), e45859. DOI:10.1371/journal.pone.0045859
18. Arnol'd, V. I. Catastrophe Theory; Springer-Verlag: Berlin, Germany, 1984; DOI:10.1007/978-3-642-96799-3
19. Poston, T.; Stewart I. Catastrophe Theory and Its Applications; Dover Publication, Inc: Mineola, New York, USA, 1996, pp. 75–89.
20. McNamara, B.; Wiensfeld, K. Theory of stochastic resonance. *Phys. Rev. A.* **1989**, 39, 4854–4869. DOI:10.1103/PhysRevA.39.4854
21. Benzi, R.; Sutera, A.; Vulpiani, A. The mechanism of stochastic resonance. *J. Phys. A: Math. Gen.* **1981**, 14, L453–L457. DOI: 10.1088/0305-4470/14/11/006
22. Wiensfeld, K.; Jaramillo, F. Minireview of stochastic resonance. *Chaos* **1998**, 8, 539–548. DOI:10.1063/1.166335
23. Gammaitoni, L.; Hänggi, P.; Jung, P.; Marchesoni, F. Stochastic resonance. *Rev. Modern Physics* **1998**, 70, 223–287. DOI:10.1103/RevModPhys.70.223
24. Avetisov V. A.; Markina, A.A; Valov, A. F. Oligomeric “Catastrophe Machines” with Thermally Activated Bistability and Stochastic Resonance. *J. Phys. Chem. Lett.* **2019**, 10, 5189–5192. DOI: 10.1021/acs.jpcclett.9b01261
25. Abraham, M.J.; Murtola, T.; Schulz, R ; et al. GROMACS: High performance molecular simulations through multi-level parallelism from laptops to supercomputers. *SoftwareX* **2015**, 19–25. DOI:10.1016/j.softx.2015.06.001
26. Jorgensen, W.L.; Maxwell, D.S; Tirado-Rives, J. Development and Testing of the OPLS All-Atom Force Field on Conformational Energetics and Properties of Organic Liquids. *J. Am. Chem. Soc.* **1996**, 118, 11225–11236. DOI:10.1021/ja9621760
27. Jorgensen, W.L.; Tirado-Rives, J. Potential energy functions for atomic-level simulations of water and organic and biomolecular systems. *Proc.Natl. Acad. Sci. USA.* **2005**, 102, 6665–6670. DOI: 10.1073/pnas.0408037102
28. Jorgensen, W.L. & Tirado-Rives, J. The OPLS [optimized potentials for liquid simulations] potential functions for proteins, energy minimizations for crystals of cyclic peptides and crambin. . *J. Am. Chem. Soc.* **1988**, 110, 1657–1666. DOI: 10.1021/ja00214a001
29. Halperin, A.; Kröger, M.; Winnik, F. Poly(N-isopropylacrylamide) Phase Diagrams: Fifty Years of Research. *Angew. Chem., Int. Ed.* 2015, 54, 15342–15367. DOI:10.1002/anie.201506663
30. Hoogenboom, R. Tunable Thermoresponsive Polymers by Molecular Design. In *Complex Macromolecular Architectures: Synthesis, Characterization, and Self-Assembly*; Wiley&Sons: New York, 2011.
31. Alaghemandi, M.; Spohr, E. Molecular Dynamics Investigation of the Thermoresponsive Polymer Poly(N-isopropylacrylamide). *Macromol. Theory Simul.* **2012**, 21, 106–112. DOI:/10.1002/mats.201100071

32. Landau, L.D.; Lifshitz, E. M. Course of theoretical physics. Vol.5 Statistical physics; Pergamon Press, London, 1952.
33. Kondepudi, D.; Nelson, G. Weak neutral currents and the origin of biomolecular chirality. *Nature* **1985**, 314, 438-441. DOI:10.1038/314438a0
34. Avetisov, V. A.; Kuz'min, V.V.; Anikin. S.A. Sensitivity of chemical chiral systems to weak asymmetric factors. *Chemical Physics* **1987**, 112, 179-187. DOI:10.1016/0301-0104(87)80160-X

Supplementary Materials

S1. Simulation protocol

Morphology simulations were performed using the GROMACS simulation package. Details of the parameters used for non-bonded interactions are presented in Figure S1a. Long-range electrostatic interactions were treated using a smooth particle mesh Ewald technique. All calculations were performed in the NVT ensemble using the canonical velocity-rescaling thermostat, as implemented in the GROMACS simulation package.

A random initial configuration was used to start the simulation. To reach an equilibrated morphology, the simulation was initialized using 16,742 water molecules and one NIPMAm oligomer in a syndiotactic configuration 30 monomeric units long. These molecules were modeled inside a box measuring $5.0 \times 3.0 \times 3.0$ nm first exposed to a thermal bath at 290 K for 50 ns with a simulated time step of 0.001 ps ($n=5$ independent trajectories). The simulation was repeated in a larger box ($8.0 \times 8.0 \times 8.0$ nm), confirming that results were not influenced by box size. An image of the larger simulation box ($8.0 \times 8.0 \times 8.0$ nm) is shown in Figure S1b.

To study how the oligomers respond to a power load, system simulation was continued for an additional 150 ns ($n=2$ independent trajectories). Model error was estimated using the full width at 50% of the distribution curve maximum. Various water models (SPCE, TIP3P, TIP4P) were used, showing that results are independent of the model applied. Significant differences in the spontaneous oscillations of the end-to-end distance R_e under the critical load ($F = 400$ pN; Figure S1c) were not found.

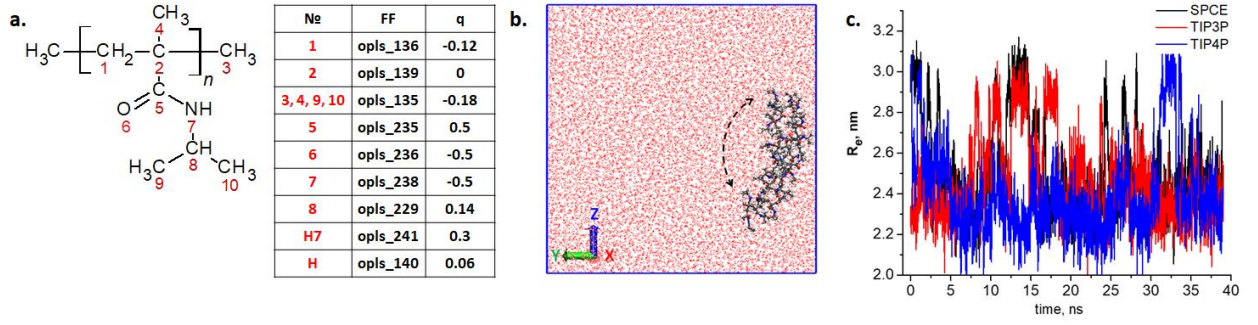


Figure S1. Simulation details. a) Non-bonded interaction parameters from the OPLS-AA force field used in the simulation; b) the YZ-plane of the simulation box ($8.0 \times 8.0 \times 8.0$ nm; 50,888 particles); and c) oscillations of the end-to-end distance R_e for various water models (SPCE, TIP3P, and TIP4P).

The simulation workflow consisted of the following:

- 1) An “open” conformation of oligo-30s-NIPMAm was obtained by equilibrating the oligomer at 290 K. This configuration of oligo-30s-NIPMAm was oriented in the YZ plane and fixed in the X dimension.
- 2) The center of mass for the first monomeric unit in the oligomeric chain was fixed using a spring potential of $k = 100 \text{ kJ/molnm}^2$. No other specific constraints for bond length or atom position were applied.
- 3) The longitudinal (compressing) load F was applied to the center of mass of the last monomer unit and directed toward the attraction point, located at the center of mass of the first monomeric unit along the vector connecting the left and right ends of the molecule. Note that the orientation of this vector changed over time because the first monomeric unit was fixed while the 30th monomeric unit was mobile.
- 4) To study stochastic resonance, an oscillating force was realized by setting a charge (+1) at one end of the oligomer and a compensative charge (−1) at the other end. An external oscillating electrical field $E = E_0 \cos \omega t$ was directed along the compressive force F . The period of the harmonic electrical field was close to the period of random fluctuation $T = 5 \text{ ns}$, and the amplitude was $E_0 = 0.2 \text{ V/nm}$.
- 5) The lateral load G was applied to the center of mass of the 16th monomer unit (the middle part of the oligo-NIPMAm). Hysteresis (Figure 4a) was observed when a lateral load was added to the system under critical compression. In this case, the vibration region (stochastic resonance) depended on increasing or decreasing the lateral load.
- 6) To represent stochastic resonance, the end-to-end distance under a compressing force F and a lateral force G that were fixed near their critical values were plotted against time.

S2. Sensing regime

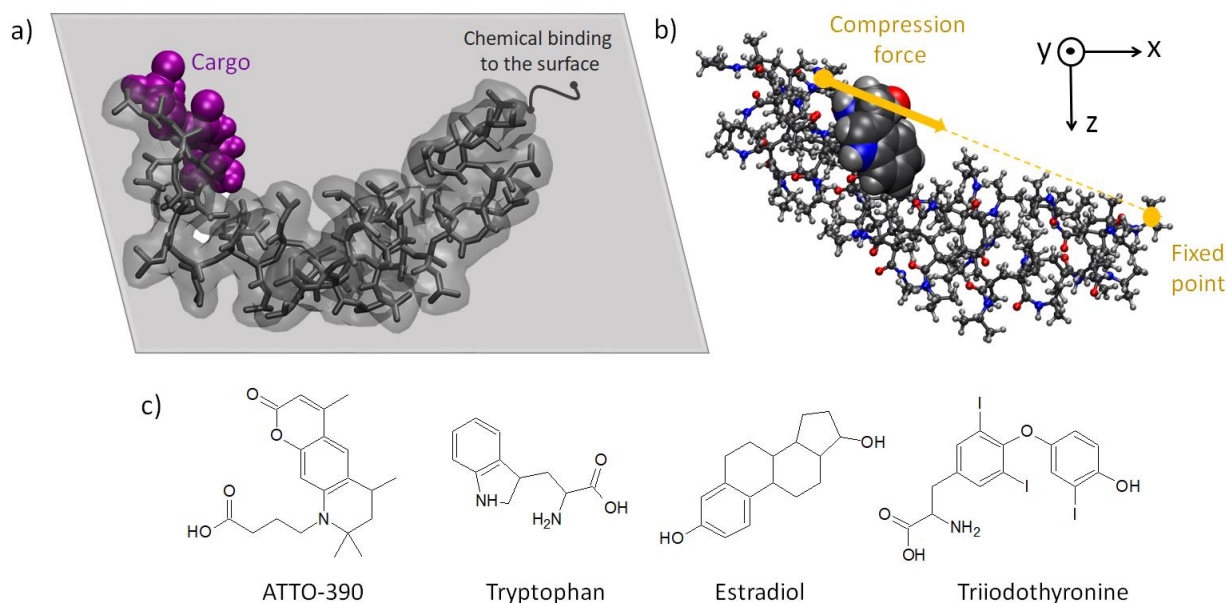


Figure S2. Model of the sensing element. a) Structure of oligo-NIPMAm, hydrophobic and hydrophilic blocks. b) Computational model of oligo-30s-NIPMAm under an applied longitudinal F load. c) Chemical structures of hydrophobic small molecules under study: the dye ATTO-390, the amino acid tryptophan, and the hormones estradiol and triiodothyronine.

To apply an additional load to the system, the following workflow was used:

- 1) An “open” conformation of oligo-30s-NIPMAm at a temperature of 290 K was oriented in the YZ plane and fixed in the X dimension (See Figures S2a and b).
- 2) Small molecules (one, two, or three) were placed in the vicinity of the oligo-NIPMAm molecule. After ~10 ns of equilibration, the small molecule was absorbed on the oligo-NIPMAm (see Figure S3 for minimum distances for various types of molecules).
- 3) The longitudinal load applied to the oligomer was then bent as described in the simulation protocol. Alternatively, the oligomer can be placed in a closed state, equilibrated at 320 K, then loaded in opposite directions. Results were not qualitatively different in this scenario.

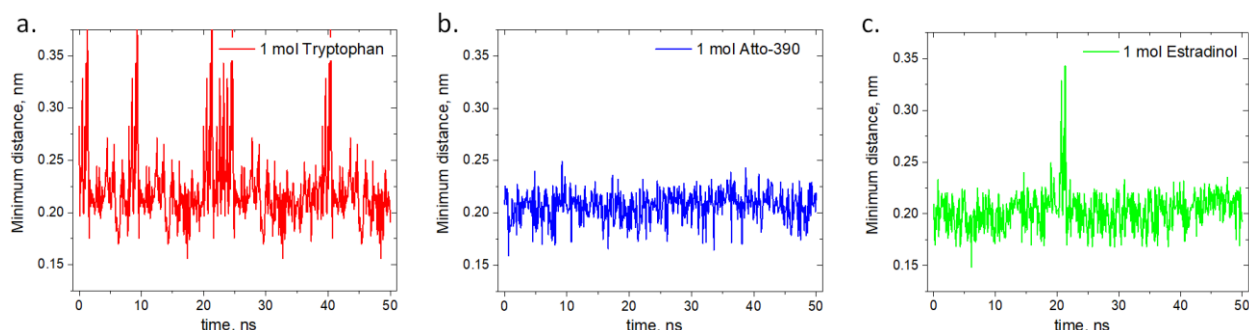


Figure S3. Adsorption of molecular cargo. The minimum distance is between any atom of oligo-NIPMA and any atom in the cargo molecule tryptophan (a), ATTO-390 (b), or estradiol (c).

The behaviors of oligo-NIPAM loaded with various types of cargos are shown in Figures S4-S6.

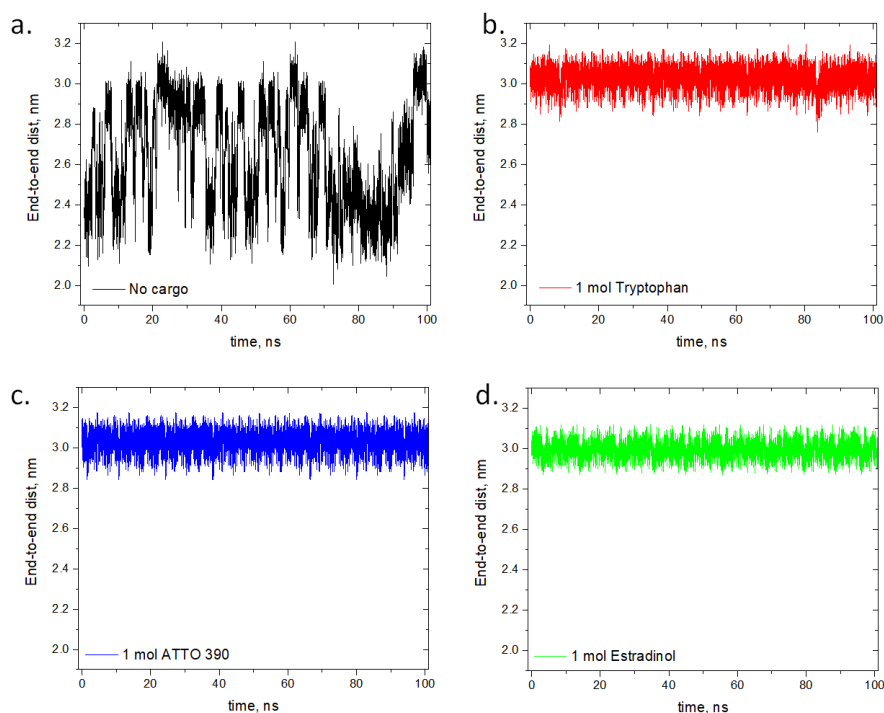


Figure S4. Sensing regime. Molecular dynamic trajectories were determined for the system under the critical compression $F = 375$ pN and without a cargo molecule (a) and with one molecule of tryptophan (b), ATTO-390 (c), or estradiol (d).

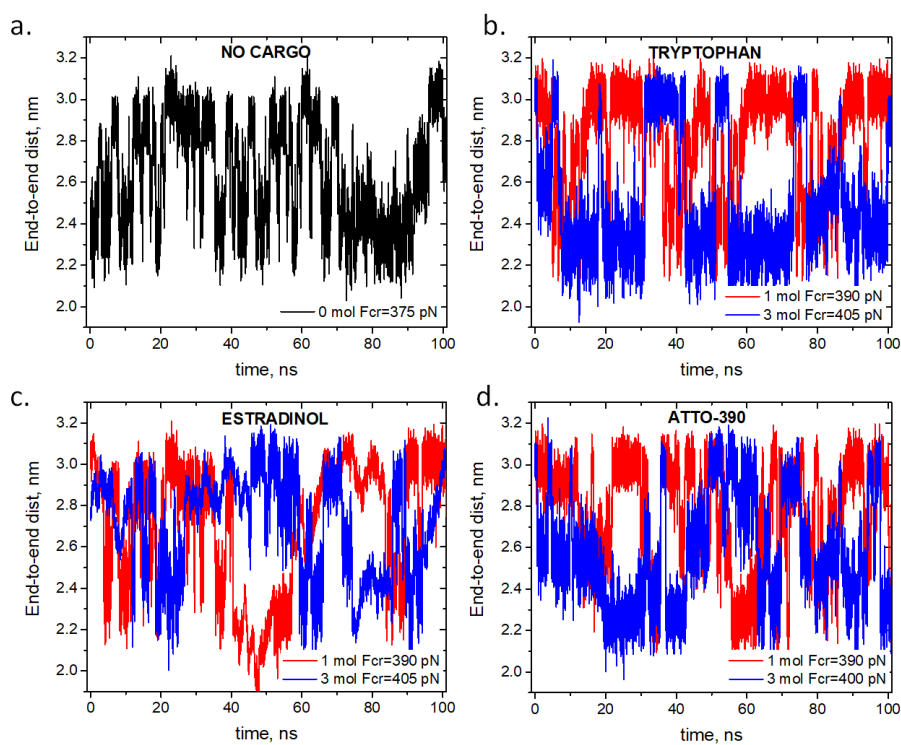


Figure S5. Molecular dynamic trajectories. The end-to-end distance of the system was determined for the system under the critical compression $F = 375\text{ pN}$ and without a cargo molecule (a) and with one or three molecules of tryptophan (b), estradiol (c), or ATTO-390 (d).

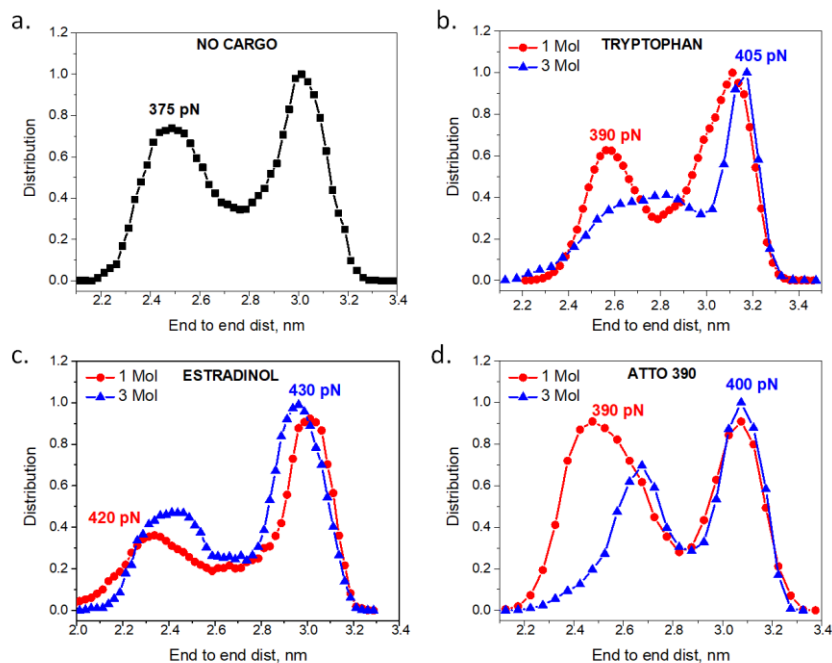


Figure S6. Spontaneous vibrations diagrams. The statistical weights of visits to the opened and closed states were determined under the critical compression $F = 375\text{ pN}$ and without a cargo molecule (a) and with one or three molecules of tryptophan (b), estradiol (c), or ATTO-390 (d).

S3. Sensitivity

The sensing regime is sensitive to the mass of the binding small molecule and its binding affinity (see Figure S7). The number of sites and the hydrogen binding affinity differed between the small molecules. Binding energies were obtained using an umbrella sampling technique.

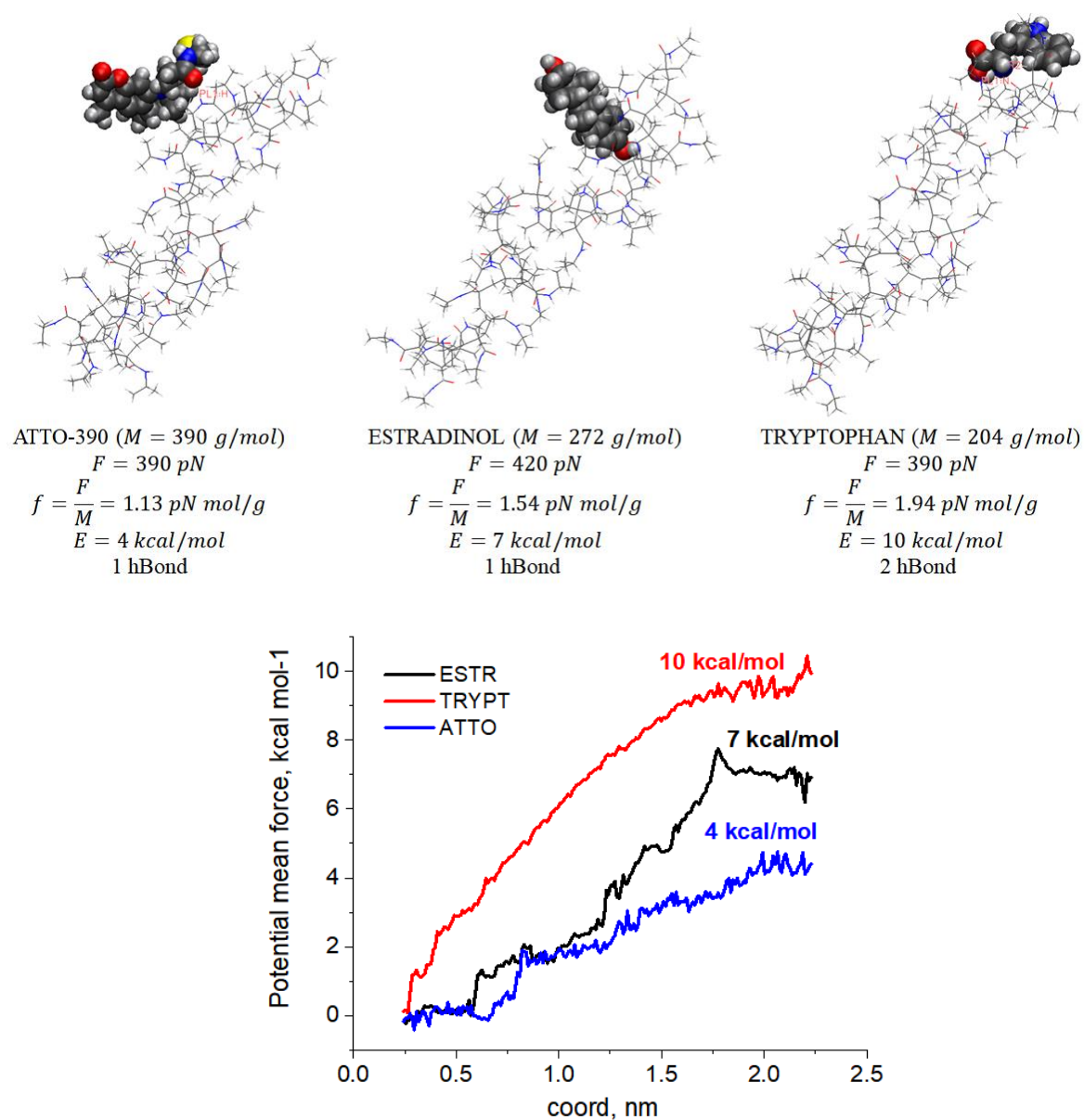


Figure S7. Binding energies and the number of hydrogen bonds in each molecule studied. The molar mass, critical force for spontaneous vibrations, critical force normalized to molar mass, binding energy, and number hydrogen bonds is shown for each molecule.